IEEE Photonics Journal
An IEEE Photonics Society Publication

A Tunable Dual-Band Metamaterial Filter Based on the Coupling Between Two Crossed SRRs

Volume 13, Number 3, June 2021

Zhijun Qiao
Xuchao Pan
Fan Zhang
Jianchun Xu

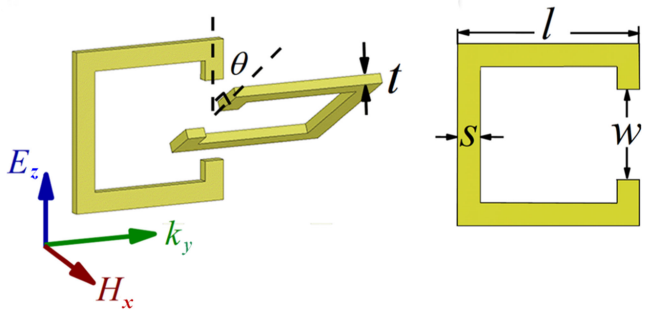

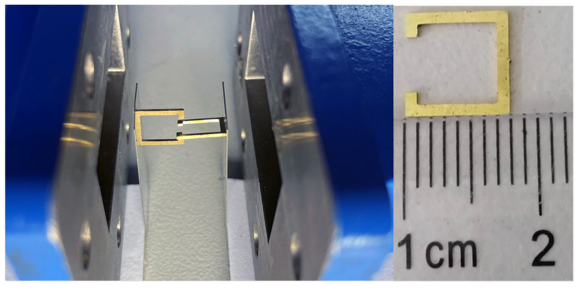

DOI: 10.1109/JPHOT.2021.3072415

A Tunable Dual-Band Metamaterial Filter Based on the Coupling Between Two Crossed SRRs

Zhijun Qiao,[1,2] Xuchao Pan,[1] Fan Zhang,[3] and Jianchun Xu [3,4]

[1]ZNDY of Ministerial Key Laboratory, Nanjing University of Science and Technology, Nanjing 210094, China
[2]Air Force Equipment Academy, Beijing 100085, China
[3]State Key Laboratory of Information Photonics and Optical Communications, School of Science, Beijing University of Posts and Telecommunications, Beijing 100876, China
[4]Beijing University of Posts and Telecommunications Research Institute, Shenzhen 518057, China

DOI:10.1109/JPHOT.2021.3072415

Manuscript received March 5, 2021; revised April 2, 2021; accepted April 6, 2021. Date of publication April 12, 2021; date of current version April 23, 2021. This work was supported in part by the Science and Technology Plan of Shenzhen City under Grant JCYJ20180306173235924 and Grant JCYJ20180306173235925. (Corresponding author: Jianchun Xu (e-mail: jianchun_xu@bupt.edu.cn).

Abstract: A tunable dual-band metamaterial filter based on crossed split-ring resonators is numerically and experimentally demonstrated. The proposed tunable metamaterial filter consists of two same metal split rings with different angles. Based on the cross-coupling between these two split rings, two stopbands are generated. Moreover, the operating frequency of the two stopbands can be tuned by changing the angle between the two split rings. In the context of numerical results, surface current distributions and electric field distributions were employed to analyze the basic principle, and the experiments were performed to demonstrate the practical effect. All results verified the tunable characteristics of the proposed metamaterial filter. This design proposes a new tunable metamaterial filter through the angle rotation.

Index Terms: Metamaterial, filter, tunable dual band.

1. Introduction

Filters are passive devices commonly used to selectively eliminate undesired information and restrain the noise of the signal in the microwave and millimeter-wave systems, which plays an important role in imaging, sensors, and communication [1], [2]. Recently, the modern communication system and other new technologies put forward higher requirements, including security, high speed, and wideband, for signal processing [3]–[5]. Therefore, the development of compact low-cost tunable filters is required to address these requirements [6], [7]. Traditional methods of achieving wideband are by using microstrip resonator, etching slot, or adopting dielectric resonator [8]–[10]. However, these methods can not completely satisfy the demands due to the complex structure, bulky volume, fixed operating bandwidth, or high cost.

Metamaterials are artificial structures that can generate many special physics properties such as negative refraction, perfect absorption, cloaking, and Doppler shift, thus attracting extensive attention [11]–[13]. The precise manipulation of electromagnetic (EM) waves and the capacity of customized design are the excellent merits of metamaterials [14]–[18]. Therefore, the existence of

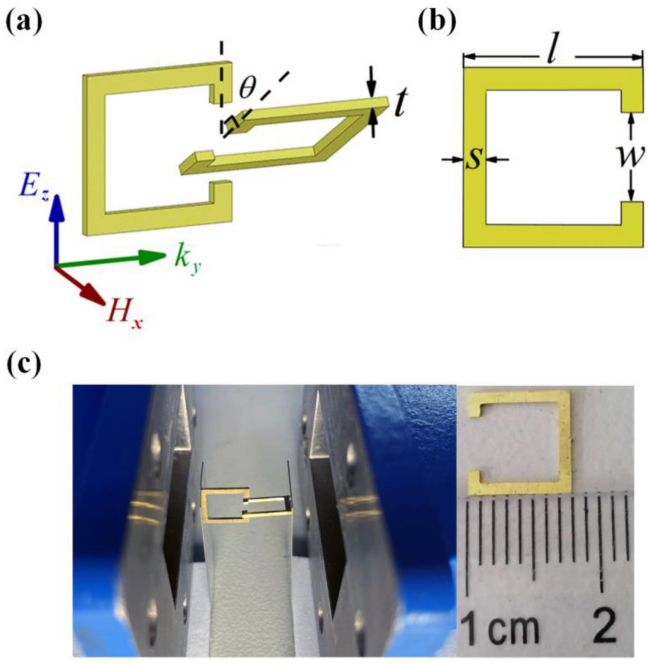

Fig. 1. Schematic diagrams of the (a) tunable filter and (b) a single split ring. (c) Photograph of the fabricated tunable filter.

metamaterials paves a new way for the designs of various tunable EM devices, including filters [19]–[22]. By changing the effective inductance or capacitance of the metamaterials through the modulations of external voltage, magnetic field, temperature, and so on, the tunable metamaterial filters can easily be achieved [23]–[27]. Except for these external field modulation methods, the mechanically tunable metamaterial filters were also reported [28]. Nevertheless, the tunning capability of bandstop metamaterial filter realized by angle rotating was scarcely reported.

Here, we propose a crossed split-ring structure for the design of a tunable dual-band bandstop filter. This compact metamaterial filter is only composed of two same crossed split rings. Due to the crossed angle between the two rings, the coupling between the two SRRs is generated when the polarized EM wave is normally incident onto the resonator. Thus, the operating frequency of the filter is modified by the rotation angle, which provides a novel design idea for actively tunable bandstop metamaterial filters.

2. Proposed Structure

Fig. 1 depicts the schematics of the proposed tunable filter which consists of two crossed split-ring resonators (SRRs). As shown in Fig. 1(a), the first SRR is fixed and its gap direction is parallel to the electric field direction of the incident EM wave. Another same SRR is oppositely located at the gap side of the first SRR. The whole SRR is made of copper. It is worth noting that the gap centers of these two SRRs are coincident. To introduce suitable coupling between two SRRs, a certain angle between the two SRRs is tuned by rotating the second SRR. Fig. 1(b) shows the top view of a single SRR, the width, side length, and gap size of this square split ring are s, l, and w, respectively. In practical applications, support frames are necessary for maintaining the angle between the two SRRs. As illustrated in Fig. 1(c), the fabricated tunable filter is supported by two thin plastic plates. The angle of θ between the two SRRs is achieved through fabricating different plastic plates as shown in Fig. 1(d). The dimensions of the SRR are $l = 8$ mm, $w = 4$ mm, $s = 1$ mm, and $t = 0.5$ mm. The wave vector direction of the incident wave is parallel to the plane loaded the first SRR.

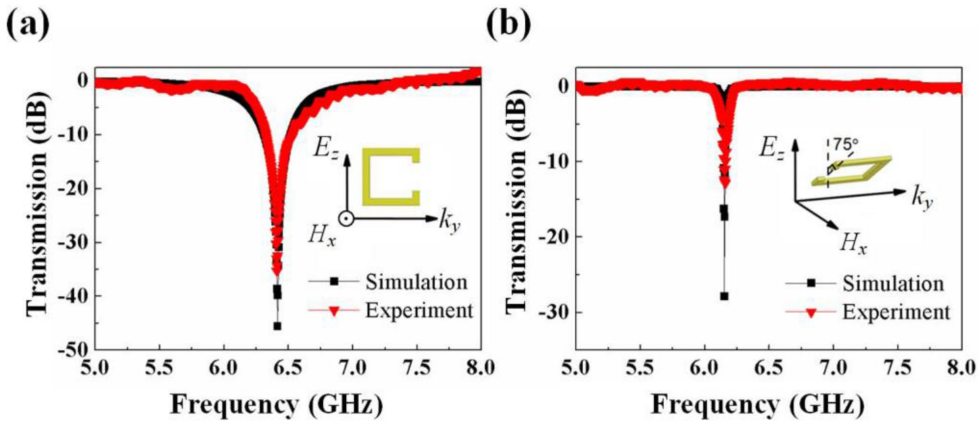

Fig. 2. Simulated and measured transmission spectrums of (a) a single first SRR and (b) a single second SRR.

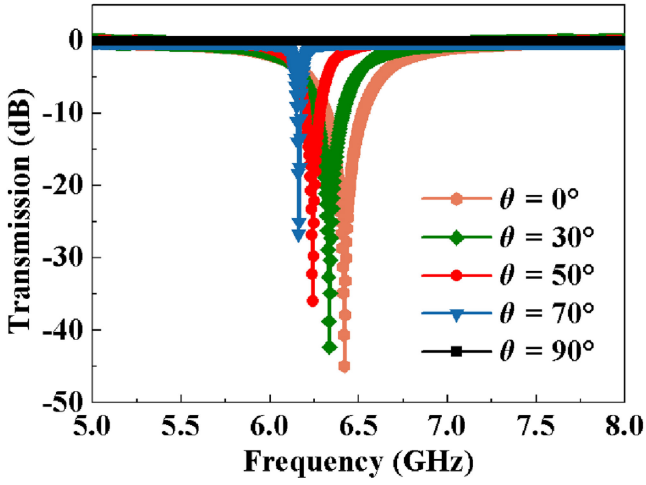

Fig. 3. Simulated transmission spectrums of the single second SRR with a series of rotation angles θ.

To further explore the basic principle in the proposed filter, numerical simulations were carried out by utilizing the commercial time-domain package CST Microwave Studio. The simulated and measured transmission spectrums of a single SRR are illustrated in Fig. 2, in which the black lines with square symbols are simulation results and the red lines with triangle symbols represent experiment results. In the experiment setting, the proposed filter supported by thin plastic plates is placed between two rectangle waveguides respectively connected to the two ports of a vector network analyzer to measure its EM performance. Fig. 2(a) shows the results of a single first SRR. In the case of normal incidence with the electric field polarized along the z-axis, an obvious resonant peak is observed around 6.42 GHz. This single SRR exhibits bandstop characteristics in the range of 6.32–6.52 GHz.

Regarding the second SRR with a rotation angle of 75°, its transmission spectrums, as shown in Fig. 2(b), also exhibit a resonant peak. But the center frequency of the resonant peak is around 6.15 GHz and obtains a redshift of 0.27 GHz. These experimental results are in good agreement with the simulation results, which demonstrate the practical possibility of realizing the tunning capability via the proposed metamaterial.

Obviously, this frequency redshift arises from the rotation angle of the second SRR. Fig. 3 depicts the simulated transmission spectrums of a single second SRR with various rotation angles θ to investigate the relationship between the phase shift and rotation angle. The existence of the rotation

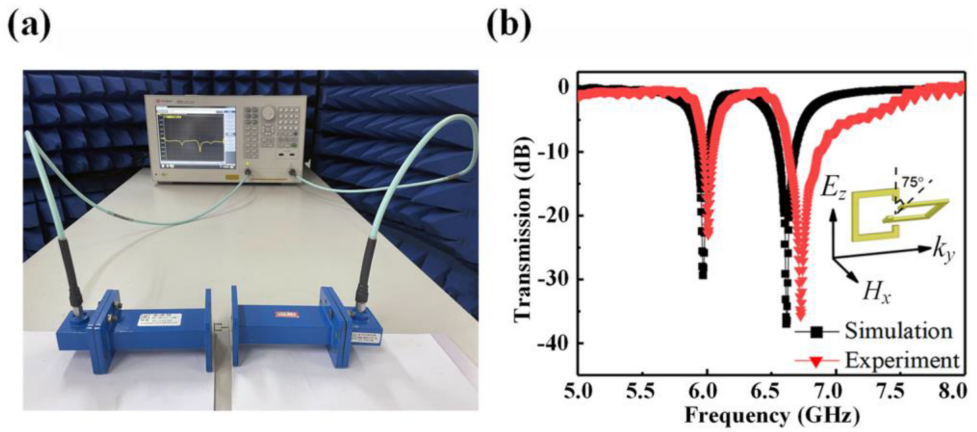

Fig. 4. (a) Measurement system. (b) Simulated and measured transmission spectrums of the proposed dual-band filter.

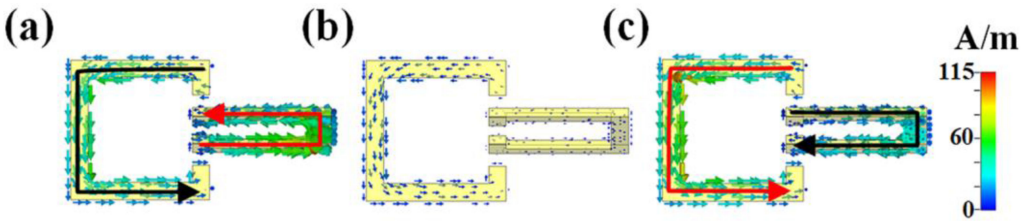

Fig. 5. Simulated surface current distributions of the proposed filter ($\theta = 75°$) at the frequencies of (a) 5.97 GHz, (b) 6.30 GHz, and (c) 6.62 GHz.

angle results in less exciting energy in the second SRR, thus decreasing the center frequency of the resonant peak. When the gap direction is vertical to the incident electric field ($\theta = 90°$), the exciting energy of the second SRR is equal to 0. Therefore, there is no resonant peak in the transmission spectrum and the SRR shows complete transparency. As the rotation angle decreases from 70° to 0°, the center frequency of the resonant peak increases from 6.16 GHz to 6.42 GHz. The equivalent circuit model can also be used to explain this phenomenon. This single SRR can be regarded as the LC circuit with inductance *L* and capacitance *C*, and its resonant frequency can be described as:

$$f = \frac{1}{2\pi\sqrt{LC}} \tag{1}$$

Because of the rotation angle, the effective distance of the gap reduced, the capacitance *C* increased, and the resonant frequency of the second SRR is thus less than the resonant frequency of the first SRR. When the second SRR is along the *x*-axis, the effective distance is equal to 0. Therefore, there is no resonant peak when the rotation angle $\theta = 90°$. As the rotation angle decreases, the effective distance increases, the capacitance decreases, and the resonant frequency increases. Particularly, the resonant frequencies of the two SRRs will be the same when the rotation angle is 0°.

From the above results, one can see that a single SRR with or without the rotation angle generates a narrow stopband centered around 6.30 GHz. In the measurement system shown in Fig. 4(a), the two SRR analyzed above are combined to form a tunable dual-band filter and the rotation angle of the second SRR is set to 75° as an example to exhibit the dual-band characteristics. The simulation result (the black solid line with square symbols) and the experiment result (the red solid line with triangle symbols) are illustrated in Fig. 4(b). Two stopbands are

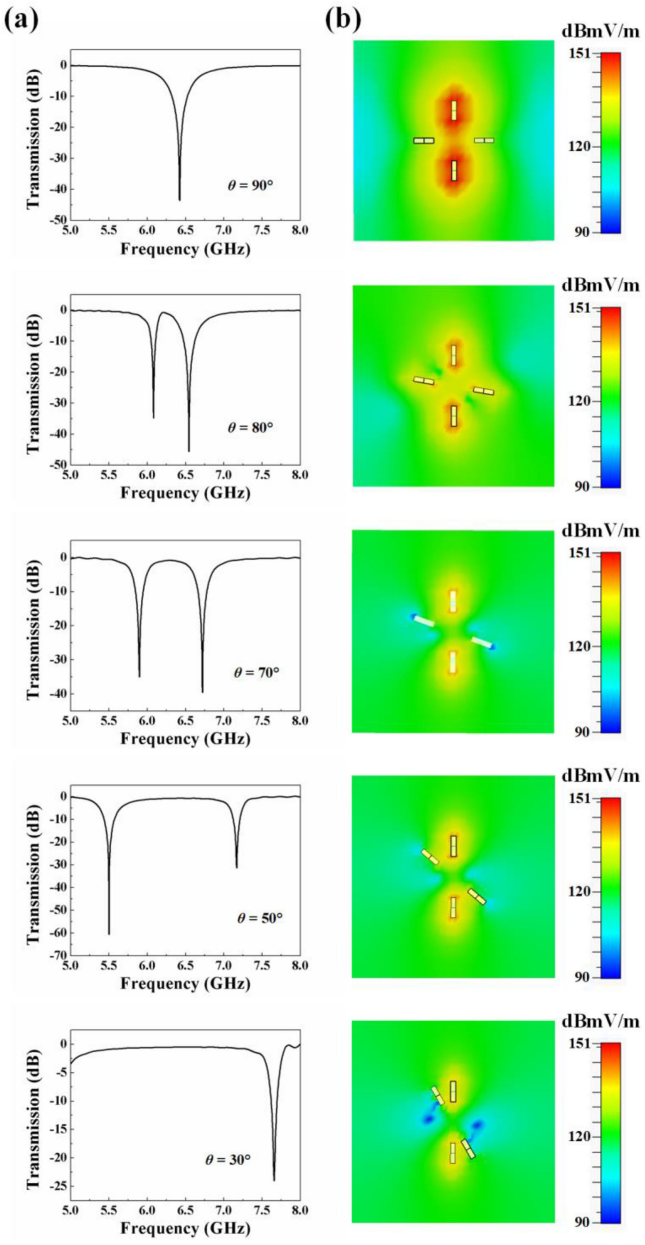

Fig. 6. Simulated transmission spectrums of the proposed tunable dual-band filter with a series of rotation angles θ and (b) corresponding electric field distributions at 6.30 GHz.

generated at 5.97 GHz and 6.62 GHz, respectively. The transmission out of the stopbands is close to 0 dB. And this transmission spectrum is similar to the spectrum of electromagnetically induced transparency analogy effect in the metamaterials. Compared to the transmission spectrums of the two single SRRs, the transparency window of the filter may be attributed to the coupling between the two SRRs. From Fig. 4, the numerical simulation curve roughly coincides with the experiment curve, which demonstrates the validity of the proposed dual-band filter.

3. Analyses and Discussions

To gain insight into the basic EM mechanism of the proposed dual-band filter, the surface current distributions at different operating frequencies are simulated and the results are shown in Fig. 5. The rotation angle of the second SRR is also set to 75°. As observed in Fig. 5, the arrows indicate the directions of the surface current flow, the strong resonances are marked by red solid lines, and the weak resonances are marked by black solid lines. At the frequency of 5.97 GHz, the surface current mainly distributes in the second SRR and the weak resonance occurs on the first SRR, which verifies that the resonance in the second SRR plays a major role at this operating frequency. Obviously, these current distributions of two SRRs are directly excited by the electric field of the incident EM wave. However, the surface current directions of these two SRRs are the opposite. Compared to the case of single second SRR, the exciting energy is reduced, thus decreasing the resonant frequency from 6.15 GHz to 5.97 GHz. A similar phenomenon occurs at 6.62 GHz as illustrated in Fig. 5(c). The different points are that the resonance in the first SRR mainly affects the EM properties of the metamaterial at this frequency and the surface current directions of the two SRRs are the same. Due to the superposition effect, the resonant frequency obtains a blueshift of 0.2 GHz compared with the condition of the single first SRR. The low-frequency resonant peak has a redshift and the high-frequency resonant peak has a blueshift. Thus, the original position of stopband generated at around 6.30 GHz appears a transparency window. As depicted in Fig. 5(b), only a little surface current distributes in the filter, which demonstrates the high out-band rejection.

According to the previous analyses, it can be inferred that the two resonant peaks of the two SRRs are both affected by the rotation angle θ. Therefore, the tunable filter has the potential to modify the stopbands by changing the rotation angle. Fig. 6 illustrates the simulated transmission spectrums and corresponding electric field distributions of the tunable filter with various rotation angles. The frequency of the observed electric fields is set at 6.30 GHz to investigate the tunning process of the stopbands. When the rotation angle $\theta = 90°$, only the first SRR is excited and forms a stopband at 6.42 GHz. The strong electric field only distributes on the first SRR, showing a high loss. As the rotation angle decreases to 80°, the electric field intensity is reduced, and the two stopbands are formed. Then the two stopbands respectively obtain redshift and blueshift with the reduction of the rotation angle. To avoid overlapping of the two SRRs, the rotation angle cannot set to 0° and the threshold value is close to 20°. While the rotation angle changes within 90° to 30°, the tunning range of the two stopbands can reach 2.5 GHz. The stopbands transform 0.045 GHz for every 1° change in angle θ. These simulation results demonstrate the tunable characteristics of the presented dual-band filter. There is only one resonant peak shown in the last transmission spectrum of Fig. 6(a). The fact is that the center frequency of another resonant peak is beyond the display range.

4. Conclusion

In summary, we proposed a tunable dual-band filter based on the crossed split-ring resonators. Excited by the incident EM wave, the two SRRs generate two near stopbands. It is numerically and experimentally demonstrated that the operating frequencies of the filter can be actively tuned by the rotation angle θ. The inherent resonant frequencies of the two SRRs are adjusted by the coupling between the SRRs. The variation range of the operating frequencies can reach 2.5 GHz as the rotation angle θ changes within 30°–90°. Moreover, the out band rejection is better than 30 dB. Owing to these characteristics, it can be believed that this work will provide a novel design idea for the tunable dual-band filters.

Acknowledgment

The authors wish to thank the anonymous reviewers for their valuable suggestions.

References

[1] A. K. Horestani, M. Duran-Sindreu, J. Naqui, C. Fumeaux, and F. Martin, "Coplanar waveguides loaded with s-shaped split-ring resonators: Modeling and application to compact microwave filters," *IEEE Antennas Wireless Propag. Lett.,* vol. 13, pp. 1349–1352, Jul. 2014.

[2] K. Bi *et al.*, "Wideband slot-coupled dielectric resonator-based filter," *J. Alloy. Comp.,* vol. 785, pp. 1264–1269, 2019.

[3] X. J. Zhai *et al.*, "Real-time automated image segmentation technique for cerebral aneurysm on reconfigurable system-on-chip," *J. Comput. Sci.,* vol. 27, pp. 35–45, 2018.

[4] J. C. Xu, K. Bi, X. J. Zhai, Y. N. Hao, and K. D. Mcdonald-Maier, "A dual-band microwave filter design for modern wireless communication systems," *IEEE Access,* vol. 7, pp. 98786–98791, Jul. 2019.

[5] S. G. Huang, B. L. Guo, and Y. A. Liu, "5G-oriented optical underlay network slicing technology and challenges," *IEEE Commun. Mag.,* vol. 58, no. 2, pp. 13–19, Feb. 2020.

[6] W. Li, N. H. Zhu, and L. X. Wang, "Continuously tunable microwave photonic notch filter with a complex coefficient," *IEEE Photon. J,* vol. 3, no. 3, pp. 462–467, May 2011.

[7] X. Y. Wang, K. Bi, Y. N. Hao, and M. Lei, "Thermally tunable dielectric resonator filter," *J. Alloy. Comp.,* vol. 749, pp. 363–368, 2018.

[8] M. Hayati and A. Lotfi, "Elliptic-function lowpass filter with sharp cutoff frequency using slit-loaded tapered compact microstrip resonator cell," *Electron. Lett.,* vol. 46, no. 2, pp. 143–144, 2010.

[9] F. F. Hu, H. X. Yi, and Z. P. Zhou, "Band-pass plasmonic slot filter with band selection and spectrally splitting capabilities," *Opt. Exp.,* vol. 19, no. 6, pp. 4848–4855, 2011.

[10] H. Hu and K. L. Wu, "A TM_{11} dual-mode dielectric resonator filter with planar coupling configuration," *IEEE Trans. Microw. Theory Techn.,* vol. 61, no. 1, pp. 131–138, Dec. 2012.

[11] K. Bi *et al.*, "Experimental demonstration of ultra-large-scale terahertz all-dielectric metamaterials," *Photon. Res.,* vol. 7, no. 4, pp. 457–463, 2019.

[12] J. C. Xu *et al.*, "A small-divergence-angle orbital angular momentum metasurface antenna," *Research,* vol. 2019, 2019, Art. no. 9686213.

[13] S. Gu, J. P. Barrett, T. H. Hand, B. I. Popa, and S. A. Cummer, "A broadband low-reflection metamaterial absorber," *J. Appl. Phys.,* vol. 108, no. 6, 2010, Art. no. 064913.

[14] K. Bi *et al.*, "All-dielectric metamaterial fabrication techniques," *Adv. Opt. Mater.,* vol. 9, no. 1, 2021, Art. no. 2001474.

[15] L. M. Si, W. R. Zhu, and H. J. Sun, "A compact, planar, and CPW-fed metamaterial-inspired dual-band antenna," *IEEE Antenn. Wirel. Pr.,* vol. 12, pp. 305–308, Feb. 2013.

[16] C. Pfeiffer and A. Grbic, "Metamaterial huygens' surfaces: Tailoring wave fronts with reflectionless sheets," *Phys. Rev. Lett.,* vol. 110, no. 19, 2013, Art. no. 197401.

[17] Z. Y. Song, Y. D. Deng, Y. G. Zhou, and Z. Y. Liu, "Tunable toroidal dipolar resonance for terahertz wave enabled by a vanadium dioxide metamaterial," *IEEE Photon. J,* vol. 11, no. 2, Apr. 2019, Art. no. 4600705.

[18] X. Q. Su *et al.*, "Broadband terahertz transparency in a switchable metasurface," *IEEE Photon. J,* vol. 7, no. 1, Feb. 2015, Art. no. 5900108.

[19] N. Liu *et al.*, "Planar metamaterial analogue of electromagnetically induced transparency for plasmonic sensing," *Nano Lett.*, vol. 10, no. 4, pp. 1103–1107, 2010.

[20] M. Z. Lu, W. Z. Li, and E. R. Brown, "Second-order bandpass terahertz filter achieved by multilayer complementary metamaterial structures," *Opt. Lett.,* vol. 36, no. 7, pp. 1071–1073, 2011.

[21] H. E. Karahan *et al.*, "Graphene materials in antimicrobial nanomedicine: Current status and future perspectives," *Adv. Healthcare Mater.*, vol. 7, no. 13, 2018, Art. no. 1701406.

[22] D. Y. Jiang, W. M. Yang, Y. J. Liu, H. L. Liu, and J. H. Teng, "The development of a wideband and angle-insensitive metamaterial filter with extraordinary infrared transmission for micro-thermophotovoltaics," *J. Mater. Chem. C,* vol. 3, no. 15, pp. 3552–3558, 2015.

[23] K. Bi, W. T. Zhu, M. Lei, and J. Zhou, "Magnetically tunable wideband microwave filter using ferrite-based metamaterials," *Appl. Phys. Lett.*, vol. 106, no. 17, 2015, Art. no. 173507.

[24] Y. Liu, R. B. Zhong, Z. Lian, C. Bu, and S. G. Liu, "Dynamically tunable band stop filter enabled by the metal-graphene metamaterials," *Sci. Rep.,* vol. 8, no. 1, 2018, Art. no. 2828.

[25] Y. Liu and L. Yi, "Tunable terahertz multichannel filter based on one-dimensional superconductor-dielectric photonic crystals," *J. Appl. Phys.,* vol. 116, no. 22, 2014, Art. no. 223102.

[26] Z. L. Han, K. Kohno, H. Fujita, K. Hirakawa, and H. Toshiyoshi, "MEMS reconfigurable metamaterial for terahertz switchable filter and modulator," *Opt. Exp.*, vol. 22, no. 18, pp. 21326–21339, 2014.

[27] K. P. Qiu, J. Q. Jin, Z. J. Liu, F. L. Zhang, and W. H. Zhang, "A novel thermo-tunable band-stop filter employing a conductive rubber split-ring resonator," *Mater. Des.*, vol. 116, pp. 309–315, 2017.

[28] J. Liu and Z. Hong, "Mechanically tunable dual frequency THz metamaterial filter," *Opt. Commun.,* vol. 426, pp. 598–601, 2018.